Temporal patterns in radar-observed convective cell development during the 2016 monsoon onset

Temporal patterns in radar-observed convective cell development during the 2016 monsoon onset

Alex Doyle[1], Thorwald Stein[1] and Andrew Turner[1,2]

[1]*Department of Meteorology, University of Reading, Reading, UK*
[2]*National Centre for Atmospheric Science, University of Reading, Reading, UK*

Introduction

The timing of onset of the South Asian summer monsoon (hereafter referred to as monsoon) is notoriously difficult to forecast (e.g. Rao *et al*., 2019), with a standard deviation in the monsoon onset of around 8 days (Pai and Nair, 2009). This interannual variability in monsoon arrival and progression has significant ramifications for communities across India, who rely on monsoon rains to alleviate the pre-monsoon heat, as well as agricultural production (Gadgil and Gadgil, 2006).

Climatologically, the monsoon arrives in southern India (Kerala) on 1 June, before moving in a non-steady motion toward the northwest, reaching the far northwest border of India by 15 July. Parker *et al*. (2016) noted the climatologically gradual withdrawal of dry air at around 400–700hPa, originating in the desert northwest, associated with cumulus congestus clouds moistening the mid-levels during monsoon advance, thus resulting in the formation of more convection. In this way, the development of convection in successive regions during monsoon advance and the associated withdrawal of dry mid-level air to the northwest drives the monsoon forwards, perpendicular to the low-level winds. Volonté *et al*. (2020) found this competition between retreating dry subtropical air and advancing moist tropical air as detailed by Parker *et al*. (2016) to be a non-linear process, modulated through intraseasonal variability (active and break periods; Rajeevan *et al*., 2010) and the occurrence of synoptic-scale features such as a cyclonic circulation over the Arabian Sea. This results in periods of hiatus and forward jumps in the progression of the monsoon, and this non-steadiness has further consequences for predictability. Furthermore, monsoon onset at Kerala at the southern tip of India has substantial interannual variability: since 1970 the date of onset as stated by the India Meteorological Department (IMD) has fluctuated from as early as 19 May in 1990 to as late as 18 June in 1972. This interannual variability combined with the aforementioned non-steadiness of monsoon advance makes onset an inherently unpredictable phenomenon across India.

Whilst cloud development and the physical processes involved are crucial components of the monsoon, their representation in weather and climate models remains a challenge, with a dry bias over the Indian subcontinent in many climate models (Willetts *et al*., 2017). Parametrisations of convection are a dominant source of error in global models (Sherwood *et al*., 2014) and suffer from historical undersampling of monsoon clouds in observations to help constrain these models. Here, using IMD Doppler weather radar observations at 12 sites across the country, we assess the large-scale temporal patterns and local cloud fields associated with monsoon onset in 2016, compared to the increase in local rainfall.

Specifically, in this article we will focus on:

1. The monitoring of convective clouds using radars and the definition of monsoon onset.
2. What did monsoon advance look like in 2016 and what large-scale dynamical changes were associated with monsoon onset and progression?
3. What is the observed temporal pattern of radar-derived convective cell coverage in the days and weeks leading up to and following monsoon onset and how does this compare with precipitation? Furthermore, how does this differ by region?

Radar data and monsoon onset definition

Indian Doppler radar data

This study aims to build a spatial representation of how the monsoon onset presents itself in terms of convective development. In order to analyse any regional differences, we consider 12 Doppler radars (Table 1), part of the IMD network. Sixteen radars with 2016 monsoon season data were made available to INCOMPASS (Turner *et al*., 2020), but two of these radars did not have data for June, thus not fully capturing the monsoon onset. A further two radars were missing substantial amounts of data from the days around monsoon onset in the region, and so were not analysed for this study. The 12 remaining radars are all S-band with the exception of New Delhi (C-band), and have a temporal sampling of 10 min between radar volume scans. All radars have similar beamwidths (0.93°–1.00°) and elevation angles (see Table 1), with similar or identical scanning strategies. There is some disparity in the gate size between different radars, varying between 250m and 1000m for Patna and Karaikal respectively. All radars were calibrated prior to analysis using clutter reflectivity and Global Precipitation Measurement (GPM) radar overpasses following the methodology of Warren *et al*. (2018) and Louf *et al*. (2019).

In order to study the height of clouds during monsoon onset we reconstruct a 3-D Cartesian grid of reflectivity data for each radar between 2 and 16km above the surface. The method is described concisely here for reasons of space, but the procedure is similar to that of Kumar *et al*. (2013), where it is described in more detail. Two kilometres is above any ground contamination and safely below the freezing level (brightband) region. The 16km maximum height is chosen to maximise the range of echo-top height retrievals: the upper edge of the beam associated with the maximum elevation angle of 21° reaches 16km at 40km range. Any clouds penetrating above this level are set to a maximum of 16.5km but may represent clouds deeper than this. A horizontal resolution of 1km × 1km matches the broadest gate size of any of the radars within 100km and vertical grid spacing is 0.5km. The vertical profile of reflectivity is calculated for each horizontal grid point by interpolating between the separate elevation scans. Once the 3-D grid of reflectivity is obtained, the Steiner *et al*. (1995) convective/stratiform classification is implemented using the reconstructed reflectivity at 2km height to identify convective pixels. A convective region is then any set of connected convective pixels using

4-connectivity. A convective pixel at 2km is assumed convective throughout the vertical profile, similarly to Kumar *et al*. (2013).

Each Cartesian pixel for each radar volume scan is given an echo-top height (ETH) based on the maximum height of the 10dBZ level. This threshold is chosen to be as low as possible but above the minimum sensitivity of all radars at 100km (see Table 1). Finally, the cell-top height (CTH) is determined as the maximum ETH in a convective region, where any cell greater than 4km^2 in size is considered for analysis. Here, we define cells with CTH ≥ 8km above ground level as deep cells, representing the most potent convection. Deep cells are associated with high 2km reflectivities (typically in excess of 30dBZ, not shown). We also prescribe those cells with CTH ≥ 5km and CTH < 8km as cumulus congestus cells, with 2km reflectivities less than 30dBZ (light rain), and CTH in the approximate region of the tropical monsoon freezing level. Whilst we only consider a single season due to radar data availability, 2016 is considered a representative year for analysis, with 97% of average all-India rainfall and an onset data at Kerala on 8 June (7 days later than the climatological average, within one standard deviation; Pai and Nair, 2009).

Monsoon onset

The definition of monsoon onset at a particular location is not trivial. Difficulty stems from the need to avoid false monsoon onsets. For example, in 2016, southeastern India saw record-breaking amounts of rainfall on 18 May due to Cyclonic Storm Roanu, but this was not associated with the monsoon regime. However, such storms can act to help advance the northern limit of the monsoon (Krishnamurti *et al*., 1981). Furthermore, it is a misconception to think there is no rain in a region prior to monsoon arrival with consistent rain after. For example, rain-shadow regions (such as southeastern India, in the leeside of the Western Ghat mountains) will often experience long dry spells following monsoon arrival. Due to the aforementioned non-steady nature of monsoon progression associated with day-to-day as well as intraseasonal variability and regional differences, it is a complex task to objectively define monsoon onset. Purely dynamical methods make sure that onset is associated with the monsoon synoptic regime (i.e. dominant westerly winds in the lower troposphere with easterly winds in the upper troposphere) but may define onset where there is little actual rain at the surface. Statistical methods rely on rainfall but are more prone to false onsets as a result. The IMD has historically used a blend of large-scale circulation features and measured rainfall to define monsoon onset and progression in a particular year (e.g. Pai and Nair, 2009). Recently, new objective criteria were released for the monsoon onset by the IMD (Pai *et al*., 2020). This method uses IMD gridded daily rainfall data (Rajeevan *et al*., 2010) to define onset at each 1° × 1° pixel, in order to ensure rainfall in a location on the day of onset, with stricter criteria for certain regions depending on the local meteorology. Further details are provided in Pai *et al*. (2020). However, on investigation, even the new objective criteria were prone to early onset, especially for northern India.

Therefore, to define onset at each radar site, we compare the radar location against the IMD progression isochrones[1]. The requirement for the IMD isochrones is for two consecutive days with rainfall in excess of 2.5mm for at least 60% of surrounding stations, given the depth of westerlies reach 600hPa and the satellite-derived outgoing longwave radiation (OLR) is less than 200Wm^{-2} in a surrounding grid-box. The IMD takes these criteria into consideration in a subjective manner to determine the onset date (Pai and Nair, 2009). The first date at which the exact radar location is level with or behind the progression line is taken as the monsoon onset date for that radar site. The date of monsoon onset for each site is shown in Table 1.

[1]IMD onset isochrones are available at https://reliefweb.int/sites/reliefweb.int/files/resources/20161010_pr_60.pdf

Large-scale drivers of cloud development at onset

Firstly, we consider the progression of the monsoon and its rainfall in 2016, and discuss the circulation changes associated with its advance. Figure 1 shows average daily rainfall totals from the GPM Integrated Multi-satellitE Retrievals (IMERG) product (Huffman *et al*., 2015), alongside 850hPa wind vectors from ERA5 (ECMWF re-analysis; Hersbach *et al*., 2020), averaged over successive pentads (grouped 5-day periods) from mid-May to mid-July 2016. The spatial resolutions of GPM IMERG and ERA5 are 0.1° and 0.25° respectively.

In May the monsoon regime is yet to be established over India. Low-level winds are from the northwest over the land, resulting in dry air advection, and are weak in magnitude. Westerlies south of India gradually spread northwards, encompassing most of India by the end of May (Figure 1(c)). Over land (except the far south of India), these westerly winds weaken again in early June (Figure 1(d)) but continue to strengthen over the Arabian Sea (west of India). As a result, rainfall begins to build offshore from the western coast of India, as well as off the southeastern coast. This brings monsoon onset to far southeastern India in the first

Table 1

Latitude and longitude coordinates for each radar site, alongside gate size and the noise value of the radar at the outer edge of the 3-D domain (100km) after calibration. The right-most column gives the date of monsoon onset in 2016 from the IMD monsoon progression isochrones.

Site name[a]	*Latitude (°N)*	*Longitude (°E)*	*Gate size (m)*	*100km noise value (dB)*	*2016 onset date*
Karaikal	10.91	79.84	1000	3	8 June
Chennai	13.07	80.29	500	2	8 June
Machilipatnam	16.18	81.15	500	2	17 June
Vishakhapatnam	17.75	83.35	1000	0	17 June
Kolkata	22.57	88.35	500	2	17 June
Patna	25.58	85.09	250	8	19 June
Agartala	23.89	91.25	500	−1	14 June
Mumbai	18.90	72.81	300	2	20 June
Nagpur	21.10	79.06	500	6	19 June
Bhopal	23.24	77.42	500	0	21 June
New Delhi	28.59	77.22	300	−5	2 July
Patiala	30.36	76.45	500	4	2 July

[a]The elevation angles for all radars except Nagpur are 0.2°, 1.0°, 2.0°, 3.0°, 4.5°, 6.0°, 9.0°, 12.0°, 16.0° and 21.0°. Nagpur's first elevation angle is 0.5°.

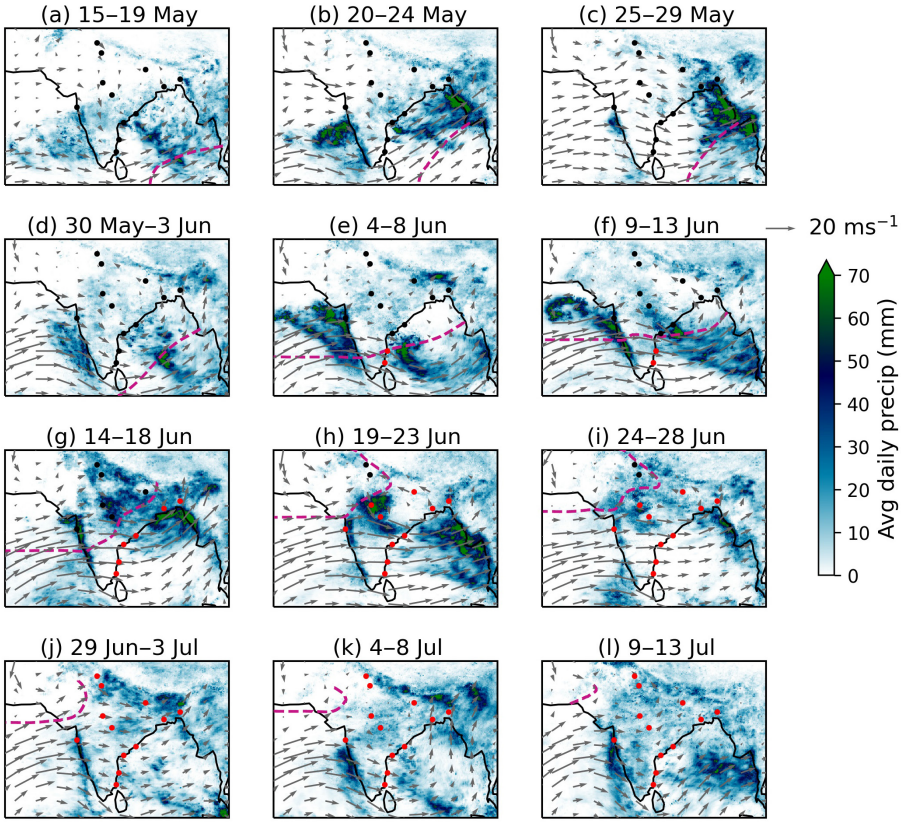

Figure 1. Pentads (5-day grouped periods) of GPM IMERG rainfall and ERA5 wind vectors at 850hPa from 15 May until 13 July, near the climatological peak of the monsoon. The locations of the 12 radar sites used (see Table 1) are marked as black dots, and are coloured red from the first pentad at which monsoon onset occurs at that site. Both the rainfall and winds are plotted as daily means averaged over the respective pentad. The purple dashed line is the northern limit of the monsoon on the last day of each pentad from the official IMD isochrones. Winds are not shown in regions above 1.5km elevation.

week of June. However, following this, a break period develops. We define a break period using rainfall over a central India zone (18–27°N, 73–82°E) and comparing to the climatological average for each day (Rajeevan *et al*., 2010 provides more details). Break periods are associated with decreased rainfall in the central India zone (and vice versa for active periods). These events can be instrumental in delaying the progression of the monsoon northwestwards (Rajeevan *et al*., 2010). The gradual movement of rainfall over western India from offshore to over land (e.g. Figures 1(e) and (f)) is associated with a clear increase in the strength of the westerly onshore winds (Fletcher *et al*., 2020). Over the Bay of Bengal (east of India), a northward-pushing wave packet associated with the Boreal Summer Intraseasonal Oscillation (BSISO) phases[2] 2 and 3 (Kikuchi *et al*., 2012) brings rainfall to much of northeastern India by mid-June (Figure 1(g)), resulting in the formation of a monsoon depression, and monsoon onset in this region. In Figures 1(g) and (h), the monsoon depression visibly tracks westwards in the 850hPa wind field, resulting in monsoon onset across the remainder of western and central India. Finally, in early July, New Delhi and Patiala in northern India experience monsoon onset as the westerly winds push sufficiently northwards. Note that New Delhi and Patiala saw significant rainfall earlier in June associated with the aforementioned monsoon depression, but this was followed by drier weather as low-level winds were still weak with a northwesterly component, and thus onset was not defined in these regions. By mid-July (Figure 1(l)), the monsoon regime is almost at its peak, with substantial and persistent precipitation over most of the country.

One major feature of the monsoon regime over South Asia is the establishment of the tropical easterly jet (TEJ). The TEJ is a thermal wind in the upper atmosphere which forms in Boreal spring due to the developing north-to-south temperature gradient between the Tibetan Plateau and the equator. It continues to increase in strength until the end of June, and is responsible for the usual westward passage of monsoon depressions (e.g. Figures 1(g) and (h)), that can be instrumental in advancing the northern limit of the monsoon through synoptic forcing (Parker *et al*., 2016). Studying mid-level relative humidity and moisture flux (see Figure 2), in general we note the gradual retreat of dry mid-level air over northwestern India throughout May and into June, as detailed by Parker *et al*. (2016). In late May (Figure 2(c)), drier air advects back into southern India which delays monsoon onset in Kerala. Into June, moisture then continues to build over most of India until the final pentad (near peak monsoon) associated with increasingly persistent convection. However, the northwestern wedge of dry air is a spatially transient feature even well into the monsoon season, sometimes retreating back into neighbouring Pakistan, and sometimes pushing back southeastward (e.g. Figures 2(h) and (k)). Intriguingly this seems to have little bearing on the monsoon advance into northwestern India in 2016. New Delhi and Patiala experience monsoon onset in Figure 2(j), associated with drier air once again encroaching from the northwest (see Figure 2(j)), but westerly winds do push north into the region at this time. This illustrates the complexities involved with predicting monsoon onset, due to the competing effects of advancing moist tropical air and dry subtropical air not always displaying a clear anti-correlation in a region.

Moisture flux vectors in Figure 2 are shown to elucidate the point that eastward moisture flux and convergence of moisture occur both sides of the northern limit of the monsoon (white dashed line), especially over the ocean. This was also noted by Parker *et al*. (2016), and therefore shows that convergence of tropical moisture-laden air alone cannot explain monsoon advance. As a result, we can expect significant convection and associated rainfall for many regions in advance of monsoon onset at a given location. This raises the importance of the additional dynamical requirement of westerly winds in the lower troposphere when defining onset.

Temporal patterns in local cloud and precipitation during monsoon advance

We now turn our attention to the convection surrounding each radar site in Table 1, comparing with local rainfall measurements from IMD 1°×1° daily gridded rainfall data (Rajeevan *et al*., 2010), and study how these observations evolve during monsoon onset at each site. Figure 3 shows 5-day running means of local precipitation and convective area for deep (CTH ≥ 8km) and cumulus congestus type cells (5 ≤ CTH < 8km). The vertical black dashed line represents the date of monsoon onset. We calculate Pearson correlation coefficients between precipitation and congestus/deep convective area, and these are labelled in Figure 3 for each site. There is a positive correlation between local rainfall and deep convective area for all sites (0.26 for New Delhi and 0.94 for Mumbai). Deep convective cells are usually responsible for

[2]Daily BSISO phase data are available at http://iprc.soest.hawaii.edu/users/kazuyosh/ISO_index/data/BSISO_25-90bpfil.rt_pc.txt

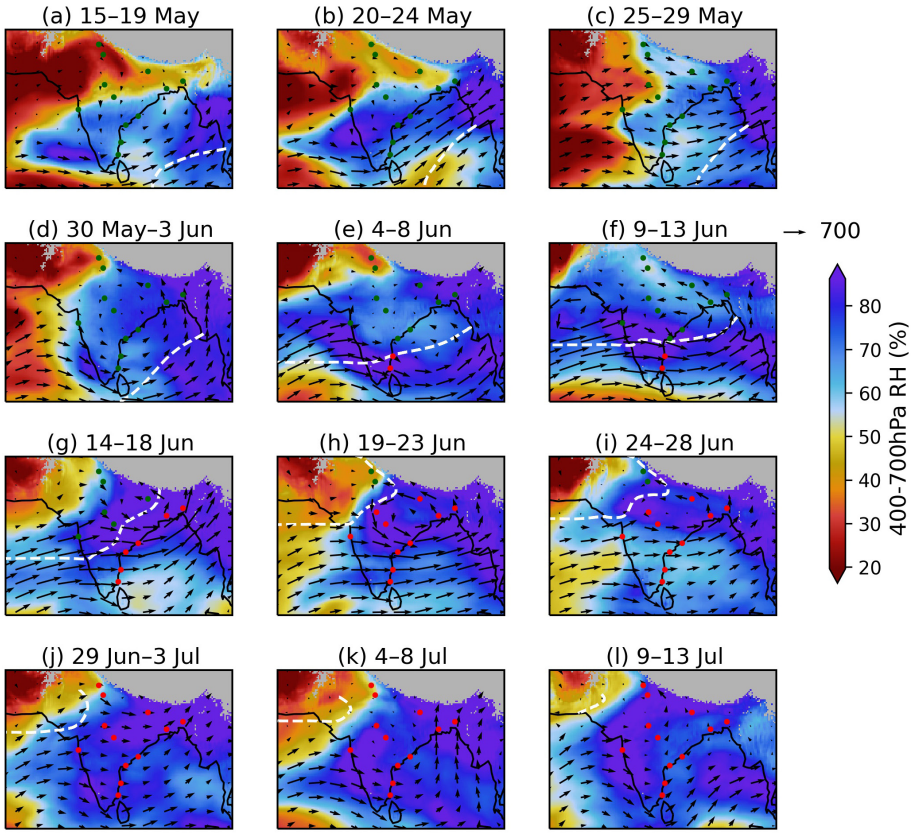

Figure 2. Same as Figure 1 but the colours show relative humidity averaged in the region 400–700hPa, alongside vertically-integrated (surface to top-of-atmosphere) moisture flux vectors ($kgm^{-1}s^{-1}$, both from ERA5. The northern limit of the monsoon is the white dashed line, and sites are coloured green before monsoon onset arrives at that location. Areas more than 2km above sea level are shaded grey.

most precipitation due to their larger average surface area and greater intensity. Two sites (Kolkata and New Delhi) show weaker correlations less than 0.5. Interestingly, both these sites show relatively higher correlations for congestus cell area. However, examining Figures 3(e) and (k) closely, the poor correlations stem from periods with a large amount of deep convection that is not reflected in the rainfall time series (e.g. Kolkata 25 June, New Delhi 8–15 July). This could be because not all deep convection at these sites is resulting in high precipitation at the surface. The area covered by congestus-type cells is significantly less compared to deep cells, resulting in a weaker correlation for most sites, but still is positively correlated with precipitation for all regions (as high as 0.92 in Mumbai). The strength of this correlation for Mumbai is likely associated with the predominance of shallow precipitating convection over the western coast of India (Utsav *et al*., 2017). It follows that an increase in deep cell coverage is usually associated with a smaller increase in congestus cell coverage. This suggests that at 5-day resolution, monsoon onset is associated with an approximately simultaneous increase in cells of multiple levels. This is in contrast to a progressive deepening of cells on this timescale, as one might infer from the Parker framework (Parker *et al*., 2016) of congestus convection moistening the mid-level troposphere, allowing deeper clouds to form as the monsoon arrives in a region.

We recall that onset is defined based on sufficiently low OLR (i.e. cold cloud tops associated with deep convection) and at least two consecutive days of 2.5mm observed precipitation. Therefore, as one might expect, monsoon onset is associated with a defined peak in precipitation and cell coverage on or a few days prior to the IMD-defined monsoon onset date in Figure 3. However, it is immediately obvious that for most sites, there is a significant amount of convection prior to the monsoon, associated with pre-monsoon rainfall, making purely observations-based definitions of onset difficult. Some sites, such as Mumbai, Nagpur and Bhopal in central west and northern India, show a more pronounced increase in rainfall from pre- to post-monsoon. Other locations show a more complex picture with significant amounts of pre-monsoon convection and rainfall. However, if a composite of several seasons of data could be considered, the temporal patterns in Figure 3 for these sites may become more meaningful. Nonetheless, the exact date of monsoon onset should not be taken too literally, owing to the high-frequency variability in rainfall associated with monsoon initiation. Furthermore, due to the definition of monsoon onset date being a hybrid of large-scale dynamical changes and measured rainfall, neither of these properties in isolation can be fully linked to the onset date. For example, some sites (e.g. Karaikal, Vishakhapatnam, Bhopal, New Delhi) show the maximum in deep cell coverage associated with onset at that location occurring a day or two in advance of the maximum in rainfall associated with onset. Intraseasonal variability associated with the BSISO is likely responsible for the high frequency variability in rainfall for most sites even after monsoon onset. Southeastern India, due to being in a rain shadow region, is prone to periods of near-zero convection and rainfall even after monsoon onset. In contrast, northern India experiences periods of plentiful convection pre-monsoon owing to active periods and monsoon depressions in June.

One interesting abnormality is the presence of significant early June (pre-onset) convection in Bhopal and Nagpur (Figures 3(i) and (j)) that is not associated with any substantial precipitation (Mumbai shows a similar signal though it is not quite as evident). However, pre-monsoon convection in other regions does result in rainfall. Further analysis with satellite data might be able to inform of the nature of this seemingly non-precipitating convection.

Conclusions

The progression of the South Asian summer monsoon is a complex and non-steady phenomenon (Volonté *et al*., 2020). As a result, it remains a relatively unpredictable area of meteorology, yet forecasts of monsoon onset in a particular region have importance for more than a billion people. Here, we have analysed the monsoon progression in 2016 from a large-scale perspective, and using a network of operational Doppler radars, analysed convective cell area in the weeks before and after monsoon onset at each respective location, comparing against local precipitation. The main conclusions from this study are as follows:

- Monsoon onset date is difficult to define objectively for specific locations. It is associated with an increase in westerly winds bringing moist tropical air, and the gradual retreat of dry mid-level air, as well as an increase in precipitation.
- The area covered by deep and congestus type cell populations correlates well with precipitation throughout monsoon onset for all sites, with only a few irregularities (e.g. Bhopal in early June). This shows that the rainfall is dominated by convective activity across all regions. Onset appears to be associated with a simultaneous increase in all types of cells as opposed to congestus gradually giving way to deep cells.

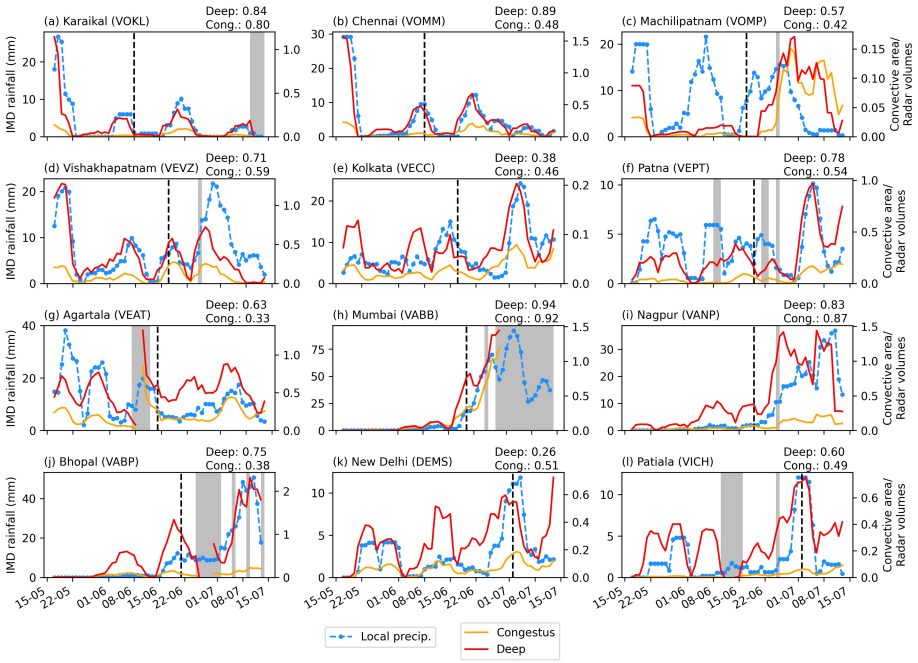

Figure 3. 5-day running means (centred on the date shown) of local precipitation from IMD 1°×1° gridded daily precipitation (spatially averaged for the nearest five grid boxes). Also shown is the daily sum of deep (CTH ≥ 8km) and congestus (5 ≤ CTH < 8km) convective area for each day (normalised by the number of radar volume scans) at each site for when data are available. Pearson product–moment correlation coefficients of precipitation against deep and congestus cell area over the time series are labelled for each site in the top right corner. Grey shaded regions are days with 0 radar volume scans for that site and are not included in the correlation. The vertical black dashed line represents the day of onset for that site, as given in Table 1.

- Mumbai, Bhopal and Nagpur show a clear increase in the amount of convection and rainfall after monsoon onset in their respective regions.
- The complexities in the clarity of onset for most other sites may be a result of their local environment (e.g. southeastern India rain shadow, northern India pre-monsoon rainfall from monsoon depressions.)

The convective cell time series examined here have been shown to be linked to local precipitation as well as the large-scale environment that they are embedded within when considering 2016 alone. However, analysing these temporal patterns across multiple years would be valuable. It is a big effort to expand such observational studies to multiple years due to the large volume of data and amount of processing time it would require, but this would be very beneficial in building up a more robust climatological picture, if data were made available.

Acknowledgements

The authors gratefully acknowledge the agreement of India's Ministry of Earth Sciences in providing the Doppler weather radar under the INCOMPASS project, funded in India under the Monsoon Mission. This work is supported by SCENARIO, grant number NE/L002566/1. The authors declare no conflict of interest. Thanks to two anonymous reviewers whose constructive comments greatly improved the overall quality of the paper.

References

Fletcher JK, Parker DJ, Turner AG *et al*. 2020. The dynamic and thermodynamic structure of the monsoon over southern India: new observations from the INCOMPASS IOP. *Q. J. R. Meteorolog. Soc.* **146**: 2867–2890.

Gadgil S, Gadgil S. 2006. The Indian monsoon, GDP and agriculture. *Econ. Polit. Wkly.* **41**: 4887–4895. https://www.jstor.org/stable/4418949 [accessed 2 March 2021].

Hersbach H, Bell B, Berrisford P *et al*. 2020. The ERA5 global reanalysis. *Q. J. R. Meteorolog. Soc.* **146**: 1999–2049.

Huffman GJ, Bolvin DT, Nelkin EJ. 2015. Integrated Multi-satellitE Retrievals for GPM (IMERG) technical documentation. https://docserver.gesdisc.eosdis.nasa.gov/public/project/GPM/IMERG_doc.06.pdf [accessed 2 March 2021].

Kikuchi K, Wang B, Kajikawa Y. 2012. Bimodal representation of the tropical intraseasonal oscillation. *Clim. Dyn.* **38**: 1989–2000.

Krishnamurti TN, Ardanuy P, Ramanathan Y *et al*. 1981. On the onset vortex of the summer monsoon. *Mon. Weather Rev.* **109**: 344–363.

Kumar VV, Jakob C, Protat A *et al*. 2013. The four cumulus cloud modes and their progression during rainfall events: a C-band polarimetric radar perspective. *J. Geophys. Res. Atmos.* **118**: 8375–8389.

Louf V, Protat A, Warren RA *et al*. 2019. An integrated approach to weather radar calibration and monitoring using ground clutter and satellite comparisons. *J. Atmos. Ocean. Technol.* **36**: 17–39.

Pai DS, Nair RM. 2009. Summer monsoon onset over Kerala: new definition and prediction. *J. Earth Syst. Sci.* **118**: 123–135.

Pai DS, Bandgar A, Devi S *et al*. 2020. CRS Research Report. New normal dates of onset/progress and withdrawal of southwest monsoon over India. https://internal.imd.gov.in/press_release/20200515_pr_804.pdf [accessed 2 March 2021].

Parker DJ, Willetts P, Birch C *et al*. 2016. The interaction of moist convection and mid-level dry air in the advance of the onset of the Indian monsoon. *Q. J. R. Meteorolog. Soc.* **142**: 2256–2272.

Rajeevan M, Gadgil S, Bhate J. 2010. Active and break spells of the Indian summer monsoon. *J. Earth Syst. Sci.* **119**: 229–247.

Rao SA, Goswami BN, Sahai AK *et al*. 2019. Monsoon mission a targeted activity to improve monsoon prediction across scales. *Bull. Am. Meteorol. Soc.* **100**: 2509–2532.

Sherwood SC, Bony S, Dufresne JL. 2014. Spread in model climate sensitivity traced to atmospheric convective mixing. *Nature* **505**: 37–42.

Steiner M, Houze RA, Yuter SE *et al*. 1995. Climatological characterization of three-dimensional storm structure from operational radar and rain gauge data. *J. Appl. Meteorol.* **34**: 1978–2007.

Turner AG, Bhat GS, Martin GM *et al*. 2020. Interaction of convective organisation with monsoon precipitation, atmosphere, surface and sea: the 2016 INCOMPASS field campaign in India. *Q. J. R. Meteorolog. Soc.* **146**: 2828–2852.

Utsav B, Deshpande SM, Das SK *et al*. 2017. Statistical characteristics of convective clouds over the Western Ghats derived from weather radar observations. *J. Geophys. Res. Atmos.* **122**: 10050–10076.

Volonté A, Turner AG, Menon A. 2020. Airmass analysis of the processes driving the progression of the Indian summer monsoon. *Q. J. R. Meteorolog. Soc.* **146**: 2949–2980.

Warren RA, Protat A, Siems ST *et al*. 2018. Calibrating ground-based radars against TRMM and GPM. *J. Atmos. Ocean. Technol.* **35**: 323–346.

Willetts PD, Marsham JH, Birch CE *et al*. 2017. Moist convection and its upscale effects in simulations of the Indian monsoon with explicit and parametrized convection. *Q. J. R. Meteorolog. Soc.* **143**: 1073–1085.

Correspondence to: A. Doyle

a.j.doyle@pgr.reading.ac.uk

doi: 10.1002/wea.3969